Finite-temperature phase diagram of nonmagnetic impurities in high-temperature superconductors using a $d=3$ tJ model with quenched disorder

Michael Hinczewski[1] and A. Nihat Berker[1,2,3]
[1]*Feza Gürsey Research Institute, TÜBITAK-Bosphorus University, Çengelköy 34680, Istanbul, Turkey*
[2]*Department of Physics, Koç University, Sarıyer 34450, Istanbul, Turkey*
[3]*Department of Physics, Massachusetts Institute of Technology, Cambridge, Massachusetts 02139, USA*
(Received 29 June 2008; published 11 August 2008)

We study a quenched disordered $d=3$ tJ Hamiltonian with static vacancies as a model of nonmagnetic impurities in high-T_c materials. Using a renormalization-group approach, we calculate the evolution of the finite-temperature phase diagram with impurity concentration p and find several features with close experimental parallels: Away from half filling, we see the rapid destruction of a spin-singlet phase (analogous to the superconducting phase in cuprates) which is eliminated for $p \gtrsim 0.05$; in the same region for these dilute impurity concentrations, we observe an enhancement of antiferromagnetism. The antiferromagnetic phase near half filling is robust against impurity addition and disappears only for $p \gtrsim 0.40$.

DOI: 10.1103/PhysRevB.78.064507 PACS number(s): 74.25.Dw, 05.30.Fk, 71.10.Fd, 74.72.−h

The electronic properties and phase diagram of high-T_c materials are particularly sensitive to impurities—substitution of $3d$ transition elements (Zn, Ni, Co, and Fe) or other metals (Al and Ga), for the Cu atoms of the CuO_2 planes.[1] The interplay between disorder, strong antiferromagnetic correlations in the parent compound and doped charge carriers offers a window onto the nature of both the superconducting phase and the normal state above T_c. Doping by nonmagnetic ($S=0$) Zn ions provides one representative example: the most pronounced effect is the rapid destruction of the superconducting phase.[1,2] In yttrium barium copper oxide (YBCO), the transition temperature is reduced at a rate of ~ 15 K/at % of impurities so that it takes Zn concentrations of only about 6% to entirely eliminate superconductivity.[2] This is in contrast to the antiferromagnetic phase at half filling, which requires a far larger Zn concentration [about 40% in lanthanum strontium copper oxide (LSCO) (Ref. 3)] to completely suppress. The effects in the metallic region above T_c are equally surprising: nuclear-magnetic-resonance experiments have found that Zn atoms induce local magnetic moments at nearest-neighbor Cu sites[4] and enhance antiferromagnetic correlations for several lattice spacings around the impurity.[5,6] In lightly hole-doped LSCO, there have been observations of an initial increase in the Néel temperature with Zn addition and even impurity-induced reappearance of long-range antiferromagnetic order.[7,8]

In this work we model the effects of nonmagnetic impurities in high-T_c materials through a $d=3$ tJ Hamiltonian with quenched disorder in the form of static vacancies. Through a renormalization-group (RG) approach, we obtain the evolution of the global temperature vs chemical-potential phase diagram with disorder. Our results capture, in a single microscopic model, some of the major qualitative features of impurity doping in real materials: the rapid suppression of a spin-singlet phase, analogous to the superconducting phase in cuprates, the gradual reduction of the antiferromagnetic phase near half filling, and the enhancement of antiferromagnetism away from half filling for small impurity concentrations.

We consider the quenched disordered tJ model on a d-dimensional hypercubic lattice, $-\beta H=\Sigma_{\langle ij\rangle}[-\beta H_0(i,j)]+\Sigma_i \mu_i^{\mathrm{imp}} n_i$, where $-\beta H_0(i,j)=-t\Sigma_\sigma(c_{i\sigma}^\dagger c_{j\sigma}+c_{j\sigma}^\dagger c_{i\sigma})-J(\mathbf{S}_i\cdot\mathbf{S}_j-n_i n_j/4)+\mu(n_i+n_j)$ is the standard tJ model pair Hamiltonian. The static impurities at each site i occur with probability p via $\mu_i^{\mathrm{imp}}=-\infty$ and do not occur with probability $1-p$ via $\mu_i^{\mathrm{imp}}=0$.

To formulate an RG transformation for this system, we use the $d=1$ Suzuki-Takano decimation,[9–19] generalized to $d>1$ through the Migdal-Kadanoff method.[20,21] This technique, adapted for quenched random-bond disorder, has recently elucidated the phase diagrams of the quantum Heisenberg spin glass in various spatial dimensions.[18] In our case the rescaling for the $d=1$ system (with sites $i=1,2,3,\ldots$) is

$$\begin{aligned}
\mathrm{Tr}_{\mathrm{even}} e^{-\beta H} &= \mathrm{Tr}_{\mathrm{even}} e^{\Sigma_i[-\beta H_0(i,i+1)+\mu_i^{\mathrm{imp}} n_i]} \\
&= \mathrm{Tr}_{\mathrm{even}} e^{\Sigma_i^{\mathrm{even}}[-\beta H_0(i-1,i)+\mu_i^{\mathrm{imp}} n_i-\beta H_0(i,i+1)]+\Sigma_i^{\mathrm{odd}}\mu_i^{\mathrm{imp}} n_i} \\
&\simeq \left[\prod_i^{\mathrm{even}} \mathrm{Tr}_i\, e^{-\beta H_0(i-1,i)+\mu_i^{\mathrm{imp}} n_i-\beta H_0(i,i+1)}\right] e^{\Sigma_i^{\mathrm{odd}}\mu_i^{\mathrm{imp}} n_i} \\
&= \left[\prod_i^{\mathrm{even}} e^{-\beta' H_0'(i-1,i+1)}\right] e^{\Sigma_i^{\mathrm{odd}}\mu_i^{\mathrm{imp}} n_i} \\
&\simeq e^{\Sigma_i^{\mathrm{even}}[-\beta' H_0'(i-1,i+1)+\mu_{i-1}^{\mathrm{imp}} n_{i-1}]} = e^{-\beta' H'}, \qquad (1)
\end{aligned}$$

where the traces and sums are over even- or odd-numbered sites i and $-\beta' H'$ is the renormalized Hamiltonian. Anticommutation rules are correctly accounted for within segments of three consecutive sites, at all successive length scales as the RG transformation is iterated.

The algebraic content of the RG transformation is contained in the second and third lines of Eq. (1), yielding the renormalized pair Hamiltonian $-\beta' H_0'(i',j')$ through the relation: $\exp[-\beta' H_0'(i',j')]=\mathrm{Tr}_k \exp[-\beta H_0(i',k)+\mu_k^{\mathrm{imp}} n_k-\beta H_0(k,j')]$. Under the transformation the original system is mapped onto one with a more general form of the pair Hamiltonian, $-\beta H_0(i,j)=-t_{ij}\Sigma_\sigma(c_{i\sigma}^\dagger c_{j\sigma}+c_{j\sigma}^\dagger c_{i\sigma})-J_{ij}\mathbf{S}_i\cdot\mathbf{S}_j+V_{ij}n_i n_j+\mu_{ij}(n_i+n_j)+\nu_{ij}(n_i-n_j)+G_{ij}$, where the interaction constants $\mathbf{K}_{ij}\equiv(t_{ij},J_{ij},V_{ij},\mu_{ij},\nu_{ij})$ are nonuniform and dis-

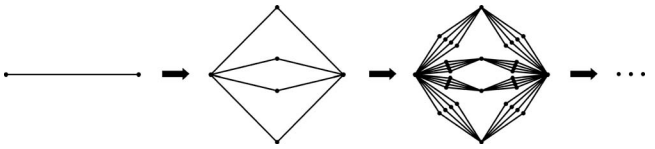

FIG. 1. Hierarchical lattice on which the $d=3$ and $b=2$ Migdal-Kadanoff recursion relations are exact.

tributed with a joint quenched probability distribution $\mathcal{P}(\mathbf{K}_{ij})$. This generalized form of the Hamiltonian remains closed under further RG transformations. Through the relation above, we can write the interaction constants $\mathbf{K}'_{i'j'}$ of the renormalized pair Hamiltonian $-\beta' H'_0(i',j')$ as a function of the interaction constants $\mathbf{K}_{i',k}$ and $\mathbf{K}_{k,j'}$ of two consecutive nearest-neighbor pairs in the unrenormalized system, $\mathbf{K}'_{i'j'} = \mathbf{R}(\mathbf{K}_{i'k}, \mathbf{K}_{kj'})$. This function $\mathbf{R}$ comes in two varieties depending on whether or not there is an impurity at site k, which we shall denote as $\mathbf{R}_0$ and $\mathbf{R}_{\text{imp}}$, respectively. Starting with a system with quenched probability distribution $\mathcal{P}(\mathbf{K}_{ij})$, the distribution $\mathcal{P}'(\mathbf{K}'_{i'j'})$ of the renormalized system is given by the decimation convolution:[22]

$$\mathcal{P}'(\mathbf{K}'_{i'j'}) = \int d\mathbf{K}_{i'k} d\mathbf{K}_{kj'} \mathcal{P}(\mathbf{K}_{i'k}) \mathcal{P}(\mathbf{K}_{kj'}) \times \{p\,\delta(\mathbf{K}'_{i'j'} - \mathbf{R}_{\text{imp}}(\mathbf{K}_{i'k}, \mathbf{K}_{kj'})) + (1-p)\,\delta(\mathbf{K}'_{i'j'} - \mathbf{R}_0(\mathbf{K}_{i'k}, \mathbf{K}_{kj'}))\}.$$

The initial condition for the RG flow is the distribution corresponding to the original system, $\mathcal{P}_0(\mathbf{K}_{ij}) = \delta(\mathbf{K}_{ij} - \mathbf{K}_0)$, where $\mathbf{K}_0 = \{t, J, -J/4, \mu, 0\}$.

The RG transformation is extended to $d>1$ through the Migdal-Kadanoff[20,21] procedure. While approximate for hypercubic lattices, the recursion relations generated by this procedure are exact on hierarchical lattices[23–25] and we shall use this correspondence to describe the RG transformation for the case $d=3$ with length rescaling factor $b=2$. The associated hierarchical lattice is shown in Fig. 1. Its construction proceeds by taking each bond in the lattice, replacing it by the connected cluster of bonds in the middle of Fig. 1, and repeating this step an infinite number of times. The RG transformation consists of reversing this construction process by taking every such cluster of bonds, decimating over the degrees of freedom at the four inner sites of the cluster, which yields a renormalized interaction between the two edge sites of the cluster. Denoting these edge sites as i' and j', and the four inner sites as $k_1, \ldots, k_4$, this decimation can be expressed as $\mathbf{K}_{i'j'} = \Sigma_{n=1}^{4} \mathbf{R}(\mathbf{K}_{i'k_n}, \mathbf{K}_{k_n j'})$. Just as in the $d=1$ case, this decimation will give, after a single RG transformation, a system with a nonuniform quenched distribution of interaction constants. We can calculate the quenched probability distribution $\mathcal{P}'(\mathbf{K}_{i'j'})$ of the renormalized system through a series of pairwise convolutions, consisting of the decimation convolution defined above for interactions in series, and a "bond-moving" convolution for interactions in parallel, using the function $\mathbf{R}_{\text{bm}}(\mathbf{K}_A, \mathbf{K}_B) = \mathbf{K}_A + \mathbf{K}_B$. In order to numerically implement the convolution, the probability distributions are represented by histograms, where each histogram is a set of interaction constants (t, J, V, μ, ν) and an associated probability. Since the number of histograms that constitute the probability distribution increases rapidly with each RG iteration, a binning procedure is used.[26] Furthermore since evaluation of the $\mathbf{R}$ functions is computationally expensive and most of the weight of the probability distributions is carried by a fraction of the histograms, we have added an additional step before the decimation convolution to increase efficiency: the histograms with the 100 largest probabilities are left unchanged while the others are collapsed into a single histogram in a way that preserves the average and standard deviation of the quenched distribution. Thus we evaluate 10^4 local decimations at each RG transformation.

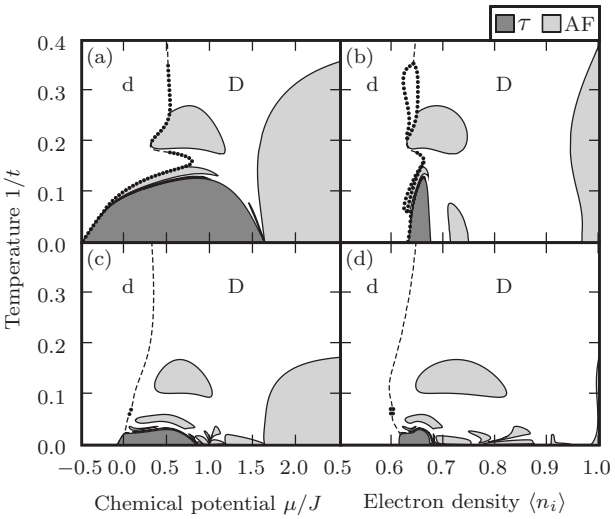

FIG. 2. Pure system ($p=0$) phase diagram of the isotropic $d=3$ tJ model (Refs. 11 and 12) for $J/t=0.444$: in terms of (a) chemical potential μ/J vs temperature $1/t$ and (b) electron density $\langle n_i \rangle$ vs temperature $1/t$. Panels (c) and (d) show the analogous phase diagrams for the uniaxially anisotropic case (Ref. 17) with $t_z/t_{xy}=0.3$, $J_z/J_{xy}=(t_z/t_{xy})^2=0.09$, and $J_{xy}/t_{xy}=0.444$. In both cases, antiferromagnetic (AF), dense disordered (D), dilute disordered (d), and τ phases are seen. The solid lines represent second-order phase transitions while the dotted lines are first-order phase transitions (with the unmarked areas inside corresponding to coexistence regions of the two phases at either side). Dashed lines are not phase transitions but disorder lines between the dilute disordered and dense disordered phases.

All thermodynamic properties of the system, in particular the finite-temperature phase diagram, can be determined from analyzing the RG flows. In the pure ($p=0$) case, the transformation described above reduces to the recursion relations derived for the $d=3$ tJ model in earlier studies,[11,12] and yields the phase diagram shown in Figs. 2(a) and 2(b) for $J/t=0.444$. Here we summarize the observed phases (for details, consult Refs. 11 and 12): near half filling ($\mu/J \to \infty$, $\langle n_i \rangle \to 1$), there is a transition with decreasing temperature from a densely filled disordered phase (D) to long-range antiferromagnetic order (AF). This AF phase persists away from half filling down to $\mu/J \approx 1.6$, or 5% hole doping. For very large hole dopings ($\gtrsim$37%), we go over

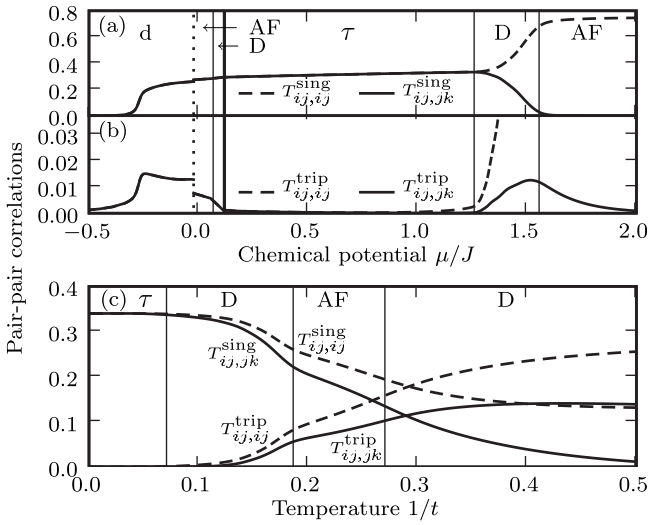

FIG. 3. On-site and nearest-neighbor singlet and triplet pair-pair correlations for the $d=3$ tJ model with $p=0$ and $J/t=0.444$. In (a) and (b) the correlations are plotted as a function of chemical potential μ/J at constant temperature $1/t=0.10$. In (c) they are plotted as a function of temperature $1/t$ at the constant electron density $\langle n_i\rangle=0.67$. The corresponding phases are indicated near the top of each plot, with solid and dotted vertical lines marking second-order and first-order phase boundaries, respectively.

into a dilute disordered phase (d) with narrow first-order coexistence regions between the d and D phases. At intermediate hole dopings of 33%–37%, a phase (τ) is found at low temperatures, flanked by an intricate lamellar structure of AF islands.

The τ phase is characterized by the formation of nearest-neighbor spin-singlet pairs, as can be understood from correlation functions calculated using the RG flows. Let us define a singlet pair-pair correlation function $T^{sing}_{ij,kl}=\langle\Delta^{sing\dagger}_{ij}\Delta^{sing}_{kl}+\Delta^{sing\dagger}_{kl}\Delta^{sing}_{ij}\rangle$, where $\Delta^{sing}_{ij}=\frac{1}{\sqrt{2}}(c_{i\downarrow}c_{j\uparrow}-c_{i\uparrow}c_{j\downarrow})$, and the analogous triplet correlation function $T^{trip}_{ij,kl}$ in terms of $\Delta^{trip}_{ij}=c_{i\uparrow}c_{j\uparrow}+\frac{1}{\sqrt{2}}(c_{i\downarrow}c_{j\uparrow}+c_{i\uparrow}c_{j\downarrow})+c_{i\downarrow}c_{j\downarrow}$. For clusters of three consecutive sites i, j, and k in the lattice, Fig. 3 shows the on-site correlations $T^{sing}_{ij,ij}$ and $T^{trip}_{ij,ij}$, and nearest-neighbor correlations $T^{sing}_{ij,jk}$ and $T^{trip}_{ij,jk}$. In Figs. 3(a) and 3(b), we see a constant-temperature slice at $1/t=0.10$ as μ/J is varied. There is a broad region of chemical potentials away from half filling, centered at the τ phase, where both the on-site and nearest-neighbor singlet correlations are strong, in contrast to the triplet correlations which are suppressed in the same region. We see similar behavior in Fig. 3(c), where the correlations are plotted as a function of temperature $1/t$ at a constant electron density $\langle n_i\rangle=0.67$. As we decrease the temperature approaching the transition into the τ phase, there is a significant increase in the singlet correlations and rapid decay of the triplet correlations. Spin-singlet liquids, i.e., the hole-doped resonating valence bond (RVB) state, have featured prominently in theories of high-T_c superconductivity (for a review, see Ref. 27). As we shall see below, the behavior of the τ phase under impurity doping is analogous to that of the superconducting phase in high-T_c materials.

Although in this study we focus on the isotropic $d=3$ model, the general features of the phase diagram discussed

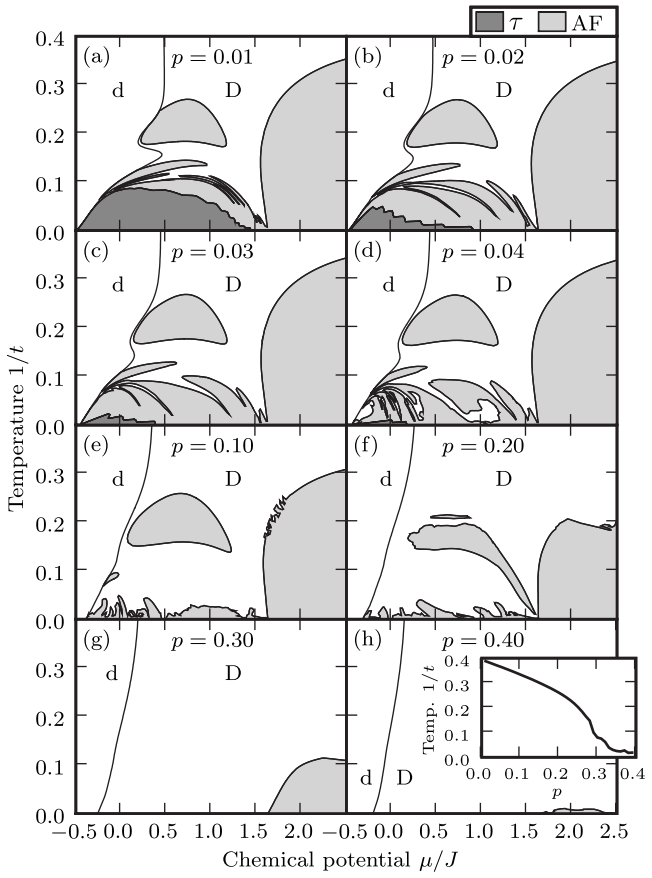

FIG. 4. Calculated phase diagrams of the $d=3$ tJ model with $J/t=0.444$ for various values of the impurity concentration p, plotted in terms of temperature $1/t$ vs chemical potential μ/J. The phases depicted in the figures are: dilute disordered (d), dense disordered (D), antiferromagnetic (AF), and τ. The inset shows AF transition temperatures for the near-half-filled system ($\mu/J=100$) as a function of p.

above persist in the case of spatial anisotropy with interactions (t_{xy},J_{xy}) along the xy planes and weaker interactions (t_z,J_z) along the z direction. Through a similar RG approach using the more complicated hierarchical lattice associated with a uniaxially anisotropic cubic lattice,[28] it was found in particular that the τ phase continues to exist in roughly the same doping range even for weak interplanar coupling.[17] A representative phase diagram with $t_z/t_{xy}=0.3$, $J_z/J_{xy}=(t_z/t_{xy})^2=0.09$, and $J_{xy}/t_{xy}=0.444$ is shown in Figs. 2(c) and 2(d). Thus the τ phase may be relevant even in the strongly anisotropic regime important for high-T_c materials, which are characterized by weakly interacting CuO_2 planes.

In Fig. 4 we show the evolution of our calculated phase diagram with increasing impurity concentration p. The τ phase is rapidly suppressed for $p=0.01$–0.04 [Figs. 4(a)–4(d)] and is no longer present by $p=0.05$. The rate at which the τ phase disappears is comparable to the reduction of T_c with nonmagnetic impurities in cuprates where typically concentrations $\approx 2\%-6\%$ (depending on dopant) are enough to eliminate superconductivity.[1,2] As the area of the τ phase recedes for these small impurity concentrations, the region it formerly occupied is replaced by a complex lamellar structure of the AF phase. We can understand this en-

hancement of antiferromagnetism through an RVB-like picture of the τ phase:[29] In the pure case, the nearest-neighbor singlets resonate in all possible arrangements along the bonds. When an impurity is added, some of these arrangements are "pruned" because the bonds adjacent to the impurity can no longer accommodate singlets. This inhibition of singlet fluctuations leads to enhanced antiferromagnetic correlations around the vacancy. Such local AF enhancement near dilute nonmagnetic impurities has been observed through NMR and nuclear quadrupole resonance (NQR) studies on Zn-doped YBCO,[5,30] and supported theoretically by finite-cluster studies of the $d=2$ Heisenberg[31] and tJ (Refs. 32 and 33) models. More dramatically, in lightly hole-doped $La_{2-x}Sr_xCu_{1-z}Zn_zO_4$ (with $x=0.017$), the Néel temperature actually increases with the addition of Zn up to $z=0.05$ before turning downwards again at higher z.[7] A similar, although smaller, effect has been found even at larger hole dopings of $x=0.115$ and 0.13 with the T_N increasing up to $z=0.0075$.[8] In the case of $x=0.13$, there is even no long-range antiferromagnetic order for the Cu spins in the Zn-free compound; it appears for $z>0.0025$. This reappearance of long-range AF order upon addition of impurities, at small hole dopings away from half filling where it does not exist in the pure case, was replicated in the $d=2$ tJ model using a self-consistent diagrammatic approach[34] and in the $d=2$ Hubbard model with the dynamical cluster approximation.[35] Thus the enhancement of the AF phase away from half filling, which we find at small impurity concentrations, is consistent with previous experimental and theoretical indications.

On the other hand, for larger concentrations of impurities, the dilution of the spins in the lattice becomes the dominant effect and eventually all long-range magnetic order is destroyed in the system. We see this in Figs. 4(e)–4(h), showing phase diagrams for $p=0.10$–0.40 and in the inset that plots the AF transition temperature as a function of p near half filling ($\mu/J=100$). In contrast to the τ phase, the AF phase around half filling is robust against impurity addition and only disappears for $p\gtrsim 0.40$. Qualitatively similar behavior has been seen in the half-filled compound $La_2Cu_{1-z}Zn_zO_4$, where Zn concentrations of $z\approx 0.4$ are required to reduce the Néel temperature to zero,[3] much larger than those needed to eliminate superconductivity in the hole-doped material.

To summarize, we have applied an RG approach to the quenched disordered $d=3$ tJ model and found the evolution of the phase diagram as a function of impurity concentration. The spin-singlet phase away from half filling is quickly destroyed through the addition of small quantities of static vacancies while antiferromagnetism in the same region is enhanced. The antiferromagnetic phase near half filling is less sensitive to impurity addition and completely disappears only at larger impurity concentration. These results all have close parallels in experimental results from cuprates. The RG method described here for dealing with quenched disorder in the tJ Hamiltonian could be generalized to more complex systems: for example, the disordered Hubbard model where the double occupation of sites is allowed through a finite electron-electron repulsion. The role of electron correlations and disorder in this system has led to interesting phase diagram predictions,[36–38] which could be further explored with RG techniques.

This research was supported by the Scientific and Technological Research Council of Turkey (TÜBITAK) and by the Academy of Sciences of Turkey.

[1] G. Xiao, M. Z. Cieplak, J. Q. Xiao, and C. L. Chien, Phys. Rev. B **42**, 8752 (1990).
[2] B. Jayaram, S. K. Agarwal, C. V. Narasimha Rao, and A. V. Narlikar, Phys. Rev. B **38**, 2903 (1988).
[3] O. P. Vajk, P. K. Mang, M. Greven, P. M. Gehring, and J. W. Lynn, Science **295**, 1691 (2002).
[4] A. V. Mahajan, H. Alloul, G. Collin, and J. F. Marucco, Phys. Rev. Lett. **72**, 3100 (1994).
[5] M. H. Julien, T. Fehér, M. Horvatić, C. Berthier, O. N. Bakharev, P. Ségransan, G. Collin, and J. F. Marucco, Phys. Rev. Lett. **84**, 3422 (2000).
[6] S. Ouazi, J. Bobroff, H. Alloul, and W. A. MacFarlane, Phys. Rev. B **70**, 104515 (2004).
[7] M. Hücker, V. Kataev, J. Pommer, J. Harass, A. Hosni, C. Pflitsch, R. Gross, and B. Büchner, Phys. Rev. B **59**, R725 (1999).
[8] I. Watanabe, T. Adachi, K. Takahashi, S. Yairi, Y. Koike, and K. Nagamine, Phys. Rev. B **65**, 180516(R) (2002).
[9] M. Suzuki and H. Takano, Phys. Lett. **69**, 426 (1979).
[10] H. Takano and M. Suzuki, J. Stat. Phys. **26**, 635 (1981).
[11] A. Falicov and A. N. Berker, Phys. Rev. B **51**, 12458 (1995).
[12] A. Falicov and A. N. Berker, Turk. J. Phys. **19**, 127 (1995).
[13] P. Tomczak, Phys. Rev. B **53**, R500 (1996).
[14] P. Tomczak and J. Richter, Phys. Rev. B **54**, 9004 (1996).
[15] P. Tomczak and J. Richter, J. Phys. A **36**, 5399 (2003).
[16] M. Hinczewski and A. N. Berker, Eur. Phys. J. B **48**, 1 (2005).
[17] M. Hinczewski and A. N. Berker, Eur. Phys. J. B **51**, 461 (2006).
[18] C. N. Kaplan and A. N. Berker, Phys. Rev. Lett. **100**, 027204 (2008).
[19] O. S. Sarıyer, A. N. Berker, and M. Hinczewski, Phys. Rev. B **77**, 134413 (2008).
[20] A. A. Migdal, Zh. Eksp. Teor. Fiz. **69**, 1457 (1975) [Sov. Phys. JETP **42**, 743 (1976)].
[21] L. P. Kadanoff, Ann. Phys. (N.Y.) **100**, 359 (1976).
[22] D. Andelman and A. N. Berker, Phys. Rev. B **29**, 2630 (1984).
[23] A. N. Berker and S. Ostlund, J. Phys. C **12**, 4961 (1979).
[24] R. B. Griffiths and M. Kaufman, Phys. Rev. B **26**, 5022 (1982).
[25] M. Kaufman and R. B. Griffiths, Phys. Rev. B **30**, 244 (1984).
[26] A. Falicov, A. N. Berker, and S. R. McKay, Phys. Rev. B **51**, 8266 (1995).
[27] P. W. Anderson, P. A. Lee, M. Randeria, T. M. Rice, N. Trivedi, and F. C. Zhang, J. Phys.: Condens. Matter **16**, R755 (2004).
[28] A. Erbaş, A. Tuncer, B. Yücesoy, and A. N. Berker, Phys. Rev. E

72, 026129 (2005).
[29] G. B. Martins, M. Laukamp, J. Riera, and E. Dagotto, Phys. Rev. Lett. **78**, 3563 (1997).
[30] Y. Itoh, T. Machi, C. Kasai, S. Adachi, N. Watanabe, N. Koshizuka, and M. Murakami, Phys. Rev. B **67**, 064516 (2003).
[31] N. Bulut, D. Hone, D. J. Scalapino, and E. Y. Loh, Phys. Rev. Lett. **62**, 2192 (1989).
[32] D. Poilblanc, D. J. Scalapino, and W. Hanke, Phys. Rev. Lett. **72**, 884 (1994).
[33] S. Odashima and H. Matsumoto, Phys. Rev. B **56**, 126 (1997).
[34] M. Kirćan and M. Vojta, Phys. Rev. B **73**, 014516 (2006).
[35] T. A. Maier and M. Jarrell, Phys. Rev. Lett. **89**, 077001 (2002).
[36] D. Heidarian and N. Trivedi, Phys. Rev. Lett. **93**, 126401 (2004).
[37] F. Fazileh, R. J. Gooding, W. A. Atkinson, and D. C. Johnston, Phys. Rev. Lett. **96**, 046410 (2006).
[38] Y. Song, R. Wortis, and W. A. Atkinson, Phys. Rev. B **77**, 054202 (2008).